NJC

Accepted Manuscript

This article can be cited before page numbers have been issued, to do this please use: J. Y. Zheng, C. W. Kim, A. U. Pawar and Y. S. Kang, *New J. Chem.*, 2016, DOI: 10.1039/C6NJ02432G.

View Article Online
DOI: 10.1039/C6NJ02432G

NJC

PAPER

Fabrication of p-Cu_2O/n-Bi-WO_3 heterojunction thin films: optical and photoelectrochemical properties†

Received 00th January 20xx,
Accepted 00th January 20xx

DOI: 10.1039/x0xx00000x

www.rsc.org/

Jin You Zheng, Chang Woo Kim, Amol Uttam Pawar and Young Soo Kang*

Transparent n-type Bi-doped WO_3 (Bi-WO_3) thin film with a thickness of *ca*. 200 nm was fabricated on fluorine-doped tin oxide (FTO) coated glass by a facile spin-coating and annealing method. The compact WO_3 layer with very smooth surface highly enhanced the transmittance of the FTO substrate. Thin p-type Cu_2O films with different morphologies were prepared on Bi-WO_3 film by electrodeposition of the same copper precursor solution with different pHs (pH 7, 9 and 11). The magnetic stirring has a limited effect on the PEC performance of the films in our deposition system. The morphologies of as-obtained films were characterized by scanning electron microscopy, which shows that the films were composed of nano-sized particles uniformly. The photoelectrochemical properties of the films were comparatively studied. Compared with the Bi-WO_3 film, the Cu_2O/Bi-WO_3 fabricated at pH 7, had better anodic photocurrent via the formation of p-n heterojunction.

1. Introduction

With the development of the world economy and the rapid growth of world population, energy needs are especially serious for not only the developing countries but also the developed countries. The non-renewable energy sources such as coal, natural gas, and fossil oil are limited; in addition, their energy combustions are causing significant human health problems and environmental contamination. Developing green and renewable energy strategies for environmental remediation and energy production is critical to solve these problems.[1] Solar energy is a very important source of renewable energy with outstanding potential compared to all other energy sources. Therefore, it is a big challenge for the utilization of solar energy, such as solar energy storage and solar energy conversion. Photocatalysis or photoelectrocatalysis assisted by semiconductors and solar energy are considered to be one of the best ways to convert the solar energy into solar fuel, which is called '*Artificial Photosynthesis*'; for examples, solar water splitting to H_2 and O_2,[2-8] and CO_2 reduction to hydrocarbon fuels such as HCOOH, HCHO, CH_4, CH_3OH, etc.[9-11] Since the artificial photosynthesis by water oxidation to evolve oxygen involves a multi-electron transfer and is much more difficult than hydrogen evolution due to thermodynamics and kinetic limitations.[12] It is a critical way to fabricate the efficient photocatalysts for water oxidation and multi-electron shuttling process to reduce CO_2 to solar fuels.

WO_3 is one of the most popular n-type photoanode materials used for oxygen evolution in photoelectrochemical (PEC) water splitting system. This is attributed to its intrinsic physical and chemical properties such as photosensitivity, good electron transport and stability against photocorrosion.[13-17] WO_3 has good hole mobility (10 cm^2 V^{-1} S^{-1}) and long hole diffusion length (150 nm),[18] which allows a relatively low photogenerated electron-hole recombination rate. However, its band gap (E_g = 2.6-2.8 eV) is relatively high and thus the light with the wavelength shorter than ca. 450 nm can be utilized to generate excitons (electron-hole pairs). In addition, the conduction band minimum of bulk WO_3 is about 0.4 V (vs NHE at pH = 0) below the hydrogen redox potential ($E_{H2/H2O}$ = 0 V);[17,19] thus, WO_3 photoanode in PEC cell can only drive half of the water-splitting reaction for oxygen evolution under an applied external bias potential or with the assistance of another special p-type photocathode, such as p-Cu_2O[20], p-Si[21] or p-$CaInP_2$[22]. The short excited-state lifetime and slow oxygen evolution reaction kinetics of WO_3 also decrease its PEC property.[23]

Cuprous oxide (Cu_2O) is a good candidate of p-type semiconductor for solar energy conversion photocatalyst due to its narrow band gap of 1.9 - 2.2 eV and suitable band edges, high photoactivity, natural abundance of copper and its low-cost production.[24,25] Cu_2O has been used as co-catalyst by forming p-n heterojunctions to enhance the photocatalytic or photoelectrochemical properties of another n-type material, such as Cu_2O/TiO_2,[26] Cu_2O/ZnO,[27] and Cu_2O/Fe_2O_3.[28,29]

For improving the PEC properties of WO_3 photoanode, the key way is to suppress the photoexcited charge recombination. There are many strategies for the suppression of charge recombination, such as the morphology control or crystal facet

Korea Center for Artificial Photosynthesis (KCAP), Department of Chemistry, Sogang University, Seoul 121-742, South Korea.
E-mail: yskang@sogang.ac.kr; Fax: (+82)-2-701-0967

† Electronic Supplementary Information (ESI) available: Experimental setup, SEM and AFM images of WO_3 film, EDS spectra, transmittance difference and photocurrents. See DOI: 10.1039/x0xx00000x

View Article Online
DOI: 10.1039/C6NJ02432G

tuning, the doping of WO_3 with different elements, the use of sacrificial agents, and the formation of heterojunctions.[1,17] Considering the energy band diagrams for WO_3 and Cu_2O as shown in Scheme 1a and 1b,[24,30,31] it is extremely suitable to create a heterojunction between WO_3 and Cu_2O. Cu_2O/WO_3 bilayer could show anodic or cathodic photocurrent properties due to two different charge transfer mechanisms in PEC system under light illumination.[24] In other words, it could be used as photoanode or photocathode in the PEC system. For showing an anodic photocurrent property (as a photoanode) from Cu_2O/WO_3 bilayer as shown in Scheme 1a, the photogenerated electron from the higher Cu_2O conduction band to the lower WO_3 conduction band, while the photogenerated holes would move from the WO_3 valence band to the Cu_2O valence band. The photogenerated hole in the valence band of Cu_2O will drive oxidation reaction such as oxidizing water to oxygen gas. For showing a cathodic photocurrent property (as a photocathode) from Cu_2O/WO_3 bilayer as shown in Scheme 1b, the photogenerated electron from the conduction band of WO_3 will combine with the photogenerated hole in the valence band of Cu_2O, while the photogenerated electron in the conduction band of Cu_2O will be used for reduction reaction such as reducing water to hydrogen gas. It should be noted that two photons are required to produce one useful electron-hole pair in second charge transfer mechanism.[24] Both two different charge transfer processes could effectively separate the electron-hole pair generated in each photocatalyst by suppressing their recombination in their respective layer.

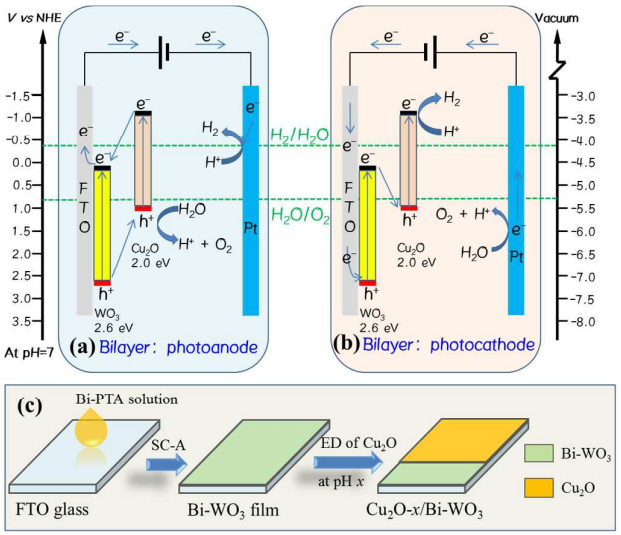

Scheme 1 Schematic illustration of (a and b) two kinds of charge transfer mechanisms for Cu_2O/WO_3 bilayer heterojunction structure under light illumination and (c) the experimental procedure for making $Cu_2O/Bi\text{-}WO_3$ bilayer film by SC-A method and followed by electrochemical deposition (ED).

In this paper, Cu_2O thin layer was electrodeposited on the Bi-doped WO_3 (Bi-WO_3) thin film prepared by a simple spin-coating and annealing (SC-A) method. These thin bilayer films on FTO substrates show high transmittance in the range of visible light. The photoelectrochemical properties of Cu_2O/Bi-WO_3 bilayer films depend on the pH of the solution for electrodeposition. The Cu_2O/Bi-WO_3 bilayer photoelectrode obtained at low pH show an enhanced anodic photocurrent. This paper can give an extended guideline on Cu_2O/WO_3 bilayer heterojunction and the other heterojunctions.

2. Experimental section

2.1 Preparation of compact Bi-WO_3 thin film by spin-coating and annealing (SC-A) method

A Bi-peroxotungstic acid (Bi-PTA) precursor solution for spin-coating was prepared as following the process. 1.5 g H_2WO_4 powder (Aldrich, 99+%) was completely dissolved in 10 mL 35 wt% H_2O_2 (Junsei, 35%) and prepared a colorless solution after constant magnetic stirring for around 6 days in a covered bottle.[16] This solution is PTA solution. Then one pure Bi metal grain was added into the preceding transparent PTA solution for 2 h reaction at room temperature, and then heating at 80 °C for 12 h until no O_2 bubbles came out. Finally, the solution for spin-coating became light yellow color but also transparent without precipitation. The viscosity and adhesive property of the solution were good for spin coating. WO_3 thin films were obtained by spin coating WO_3 precursor solution on commercial fluorine-doped tin oxide (FTO, 2 × 3 cm) coated glass (Pilkington FTO glass (TEC 8), 6~9 ohm/sq) at 1500 rpm for 20 sec by using a spin coater (spin coater ACE-200, Dong Ah Trade Corp) then followed by annealing at 500 °C for 2 h in a muffle furnace (Ajeon Heating Industrial Co., Ltd.). The spin-coating and annealing processes are very simple and the WO_3 thin film can be fabricated on a large scale.

2.2 Electrodeposition of Cu_2O thin layer on FTO glass and Bi-WO_3 film

Cu_2O was electrodeposited in a conventional three-electrode cell system using a potentiostat PL-9 (PhysioLab Co., Ltd., Korea) as we reported in the previous works.[19,32] A home-made cell was used for electrodeposition as shown in Fig. S1(ESI†). A platinum foil (1.3 × 2.5 cm) and Ag/AgCl in 3.0 M NaCl electrolyte solution were used as counter and reference electrodes, respectively. The bare FTO glass and Bi-WO_3/FTO were used as the working electrodes. The distance between the working electrode and counter electrode was determined as about 1.0 cm. The working electrode was dipped into the electrolyte solution which containing 25 mL of 0.1 M $Cu(NO_3)_2{\cdot}2.5H_2O$ (Aldrich, 99.99+%) and 3.0 M lactic acid (Kanto, 85.0~92.0% solution in water) with different pHs (pH = 7, 9 and 11) at -0.4 V for 30 min without stirring under ambient at 24 °C. The pH was adjusted by adding 4.0 M NaOH (Junsei, > 96%). The electrodeposited area was about 4 cm^2 (2 × 2 cm). For comparison, the typical Cu_2O films were also electrodeposited under the stirring condition with a magnetic stir bar at 350 rpm. All potentials reported in this work were measured with respect to Ag/AgCl electrode.

2.3 Characterization

X-ray diffraction (XRD, Rigaku miniFlex-II desktop, Cu Kα radiation with λ = 0.154056 nm) patterns were used to check crystallinity and crystal structure of the deposits. Surface and cross-sectional morphologies of the films were obtained using a

View Article Online
DOI: 10.1039/C6NJ02432G

Hitachi Horiba S-4300 scanning electron microscope (SEM) operated at 20 kV. Atomic force microscopy (AFM) measurements were carried out for thin films in a tapping mode using a Park System NX10. XEI program was used to convert acquired data into an image and to perform various analyses. Transmittances of the films were recorded on a Varian Cary 5000 UV–vis-NIR spectrophotometer. X-ray photoelectron spectroscopy (XPS: monochromator Al Kα X-ray source, K-alpha, Thermo U.K.) was used to determine the atomic state in Cu_2O and Bi-WO_3 by measuring the binding energy of the elements in the films. Photoelectrochemical measurements were conducted with potentiostat PL-9 in a conventional three-electrode system in a V-style with quartz window cell at room temperature under 1 sun (Asahi HAL-320 solar simulator, AM1.5G, Class A) illumination, employing a coiled Pt wire and an Ag/AgCl electrode as counter and reference electrode, respectively. The light intensity (1 sun) of the solar simulator is checked by a 1 sun checker CS-20. Current-potential curve was measured using linear sweep voltammogram (LSV) with a scan rate of 10 mV/s with a chopped light (on/off cycles of 1 s). Photocurrent stability were carried out by measuring the photocurrent produced under chopped 1 sun light illumination (on/off cycles of 10 s) at 0.65 V *vs* Ag/AgCl for 30 min. Electrochemical impedance spectra (EIS) was conducted with the potentiostat (VSP, Biologics). The frequency was set from 200 kHz to 0.01 Hz at open-circuit potential (E_{oc}) and the amplitude was 10 mV. A 0.5 M Na_2SO_4 aqueous solution (pH 6.3) was used as an electrolyte solution for all PEC properties checking.

3. Results and discussion

To construct a p-Cu_2O/n-WO_3 heterojunction, a simple process of the thin films fabrication was carried out as shown in Scheme 1c. The thin n-type Bi-WO_3 film was prepared by a spin-coating of Bi-PTA solution on FTO substrate and followed by annealing at high temperature. The as-obtained Bi-WO_3 thin films were used as working electrodes for electrodeposition of p-type Cu_2O thin films at different pHs (pH 7, 9, and 11). Finally, Cu_2O/Bi-WO_3 heterojunction films were obtained and used for studying the optical and photoelectrochemical performances. As shown in Fig.1 a-e, the surface of the bare commercial FTO-coated glass with thickness of around 800 nm is very rough. After fabricating the Bi-doped WO_3 layer with *ca*. 200 nm thickness onto the FTO layer by a facile SC-A method, the surface of the film becomes very smooth even similar with the commercial ITO glass as shown in our previous report.[32] The size of the particles in the Bi-WO_3 film is less than 50 nm. It is much smaller than the sizes of the particles in the WO_3 films obtained from a solution prepared by adding poly(vinyl alcohol) (PVA) in PTA solution (Fig. S2, ESI†).[16] The EDS data of Bi-doped WO_3 film shows only a little amount of Bi element (Bi:W = 1:20.4) as shown in Fig. S3 (ESI†). The photographs of the bare FTO and Bi-WO_3 film on the white paper with printed words "*Sogang Univeristy*" are shown in Fig. 1f. It can be easily observed that the transmittance of the Bi-WO_3 film is better than that of the bare FTO glass. This phenomenon can be confirmed by the corresponding transmittance spectrum as shown in Fig. 1h. The reason is that the surface of the Bi-WO_3 film is much smoother than the surface of the bare FTO glass, thus the light diffuse-reflection is suppressed greatly. Without WO_3 layer, Cu_2O films with different morphology can be directly deposited on the bare FTO glass at -0.4 V *vs* Ag/AgCl for 30 min with different pHs of the electrolyte solution such as pH 7, 9 and 11, named as Cu_2O-7, Cu_2O-9, and Cu_2O-11, respectively. Their digital photograph is shown in Fig. 1g1-3. Their transmittance becomes lower than that of the bare FTO glass as shown in Fig. 1h; it was decreased by around 10% to 50% in the visible light range as shown in Fig. S4a (ESI†). This is caused by the light absorption and reflection by the Cu_2O layer. However, after making a Bi-doped WO_3 layer on FTO, the uniform Cu_2O films can also be deposited at pH 7, 9 and 11 as the digital photograph in Fig.1g4-6; the as-obtained films were named as Cu_2O-7/Bi-WO_3, Cu_2O-9/Bi-WO_3, and Cu_2O-11/Bi-WO_3, respectively. Their transmittance was better than the Cu_2O films obtained at the same pH of the electrolyte except at pH 9 as shown in Fig. 1i. Especially, the transmittance of Cu_2O-7/Bi-WO_3 and Cu_2O-11/Bi-WO_3 was similar with the bare FTO substrate at a long wavelength range from 600 - 800 nm as shown in Fig. S4b (ESI†).

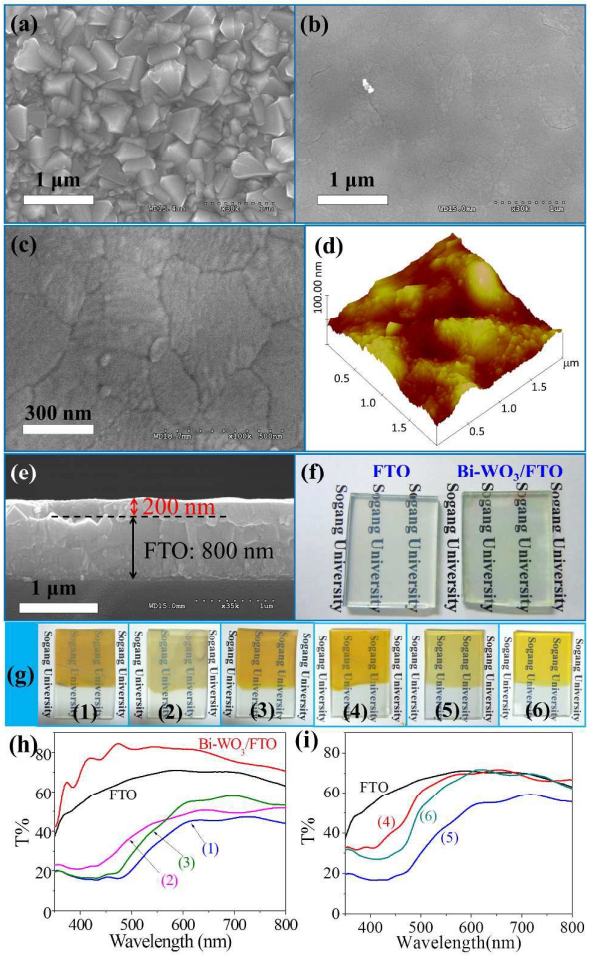

Fig. 1 (a) SEM images of the bare FTO glass; (b and c) top-view and (e) cross-sectional SEM images, (d) AFM image of the Bi-WO_3 thin film, (f) digital photographs, (g, h and i) digital photographs and transmittances of (g1 and h1) Cu_2O-7, (g2 and h2) Cu_2O-9, (g3 and h3) Cu_2O-11, (g4 and i4) Cu_2O-7/Bi-WO_3, (g5 and i5) Cu_2O-9/Bi-WO_3, and (g6 and i6) Cu_2O-11/Bi-WO_3 films on FTO substrates.

View Article Online
DOI: 10.1039/C6NJ02432G

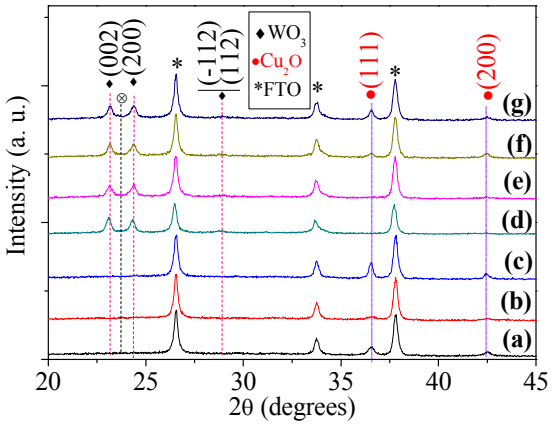

Fig. 2 XRD patterns of (a) Cu_2O-7, (b) Cu_2O-9, (c) Cu_2O-11, (d) Bi-WO_3, (e) Cu_2O-7/Bi-WO_3, (f) Cu_2O-9/Bi-WO_3 and (g) Cu_2O-11/Bi-WO_3. The absent (020) peak of WO_3 is marked by ⊗.

The corresponding XRD patterns of the as-deposited films were shown in Fig. 2. Only two main peaks at 36.56° and 42.45° can be observed in Cu_2O/FTO films, which are indexed to the (111) and (200) crystal planes of the cubic-phase Cu_2O (space group: *Pn*-3*m*; JCPDS no. 65-3288) as shown in Fig. 2(a-c), respectively.[19,32] Bi-WO_3 film shows two main peaks at 23.1° and 24.3°, which are corresponding to the (002) and (200) of the monoclinic phase WO_3 (space group: P21/n(14); JCPDS no. 43-1035) as shown in Fig. 2d, respectively.[16,33] A broad peak in the range of 2θ = 28.5-29.1° could be attributed to (-112) and (112). Interestingly, one of the characteristic (020) peak of monoclinic was absent in the position as marked in Fig. 2. XRD patterns of Cu_2O/Bi-WO_3 films in Fig. 2e-g show the combined crystal information of Cu_2O and WO_3, which indicates that the layered structure of Cu_2O/Bi-WO_3 is perfectly formed.

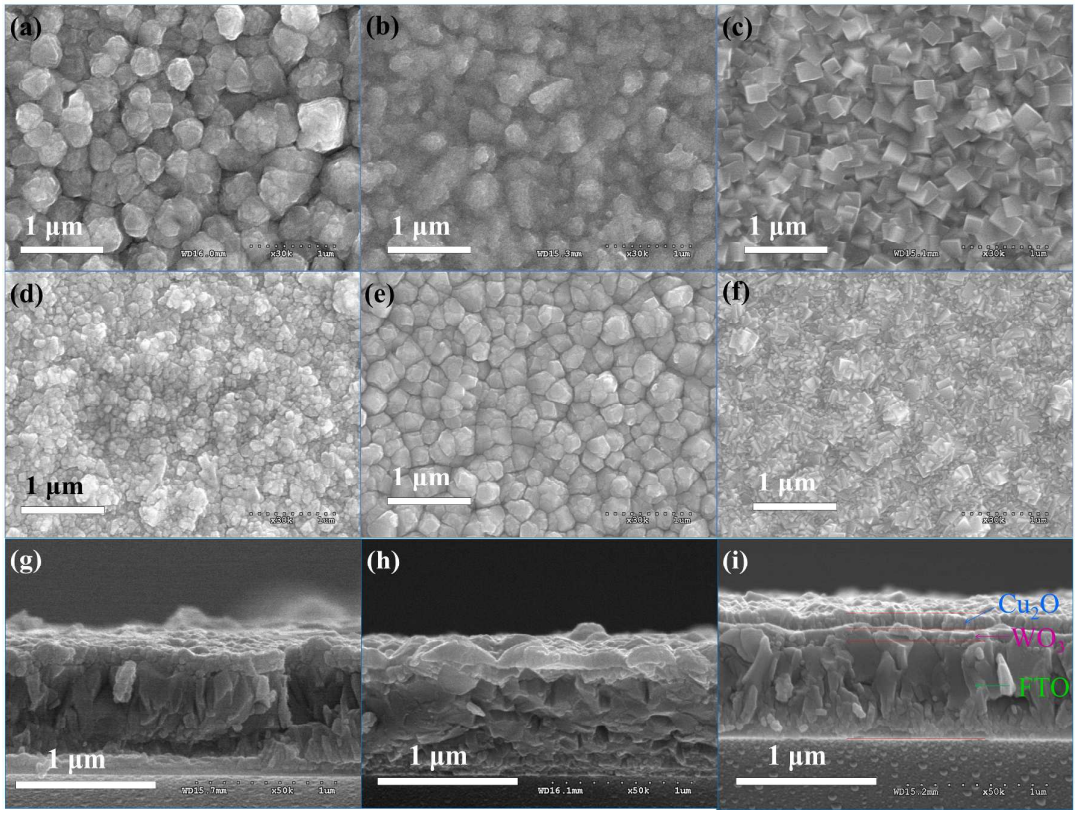

Fig. 3 Top-view and cross-sectional SEM images of the electrodeposited Cu_2O films on the bare FTO substrates and the Bi-WO_3 films at different pHs. (a) Cu_2O-7, (b) Cu_2O-9, (c) Cu_2O-11, (d, g) Cu_2O-7/Bi-WO_3, (e, h) Cu_2O-9/Bi-WO_3 and (f, i) Cu_2O-11/Bi-WO_3.

The surface morphologies of the Cu_2O layers on the bare FTO glass and the Bi-WO_3 thin film are shown in Fig. 3. SEM images of Cu_2O films as shown in Fig. 3a-c, obtained at pH 7, 9 and 11, are composed of ball-like particles, irregular particles, and cubic particles, respectively. The as-obtained Cu_2O films are uniformly covered on the substrate as the low magnification SEM images shown in Fig. S5 (ESI†). The morphologies are similar to the Cu_2O films obtained on the ITO substrate by the electrodeposition method at the same condition.[32] After the FTO glass was changed to the smooth Bi-WO_3/FTO, the morphologies of the deposited Cu_2O films are slightly different as shown in Fig. 3d-f. The Cu_2O-7/Bi-WO_3 bilayer film is more compact than Cu_2O-7 and composed of the much smaller particles. The morphology of Cu_2O-9/Bi-WO_3 is similar with that of the Cu_2O film deposited on ITO at pH7 as shown in the previous report.[32] The morphology of the Cu_2O-9/Bi-WO_3

View Article Online
DOI: 10.1039/C6NJ02432G

bilayer film is very different with that of Cu_2O-11, composed of very small cubic corners. The deposited Cu_2O films with different substrates such as FTO glass and Bi-WO_3 film are different. There are two possible reasons to explain it. First, the roughness of the two substrates is very different. Second, the surface environments of two substrates are different. The FTO film is very stable at pH 7 - 11 while the Bi-WO_3 is not so stable at the high pH condition. WO_3 is an Arrhenius acid and is known to be decomposed under neutral or basic conditions according to the reported known reactions,[34]

$$WO_3\,(s) + H_2O\,(l) \rightarrow WO_4^{2-}(aq) + 2H^+(aq) \quad (1)$$

or $$WO_3\,(s) + 2OH^-(aq) \rightarrow WO_4^{2-}(aq) + H_2O\,(aq) \quad (2).$$

WO_3 film will be slightly dissolved at the surface via the reaction 1 and/or 2. Therefore, the surface environment such as pH and presence of ionic species of Bi-WO_3 film is very different with those of the bare ITO and FTO glass substrates.

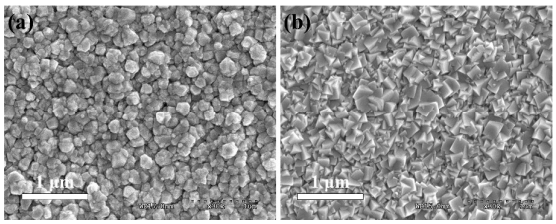

Fig. 4 Typical SEM images of the electrodeposited (a) Cu_2O-7s and (b) Cu_2O-11s different pHs with continue stirring.

To evaluate the effect of the stirring in the electrodeposition process, the typical films obtained at pH 7 and 11 with stirring, named as Cu_2O-7s and Cu_2O-11s, respectively, were carried out as shown in Fig. 4 and Fig. S6 (ESI†). With the stirring, the size of particles in the films become smaller and more irregular than those of the films obtained without stirring, which can be attributed to stirring can enhance mass transfer and reduce concentration gradient. The films are also well covered on the FTO substrates and relatively uniform under stirring condition as the low magnification SEM images shown in Fig. S6. The average surface roughnesses (R_a) of the films (10 μm × 10 μm) prepared with and without stirring are very similar as the AFM images shown in Fig. S7 (ESI†). The films obtained with stirring have relatively lower R_a than those obtained without stirring.

To determine detailed elemental information on the surface of the films, the XPS spectra of the Cu_2O-7 and Bi-WO_3 films was carried out as shown in Fig. 5 and S8 ((ESI†)). The survey scan spectra (Fig. S8 (ESI†)) confirm the presence of Cu and O in CuO film and the presence of W, O and Bi in Bi-WO_3 film, and the presence of a small amount of C in both films. Carbon could be attributed to the sample preparation (carbon sources in air) and subsequent handling, or the slightly exposed carbon tape which was used for holding samples. Both films show no substrate peaks (Sn signals from FTO), which indicates that the films are fully covered on the FTO substrate. The atomic ratio of Cu:O in Cu_2O film is about 1.3:1. The theoretical ratio of Cu:O in Cu_2O should be 2:1. The atomic ratio of Bi:W:O is about 1:17:58.9 and the W:O is ca. 1:3.5, close to 1:3. The Bi:W ratio is close to the value obtained by the EDS (1:20.4). The high oxygen element ratio in both films is attributed by the surface adsorbed hydroxide. High resolution XPS spectra of Cu2p and O1s are shown in Fig. 5a and 5b to show the purity of the Cu_2O film, which are similar with the results of Cu_2O/Cu film as shown in the previous report.[25] Some very weaker shake-up satellite peaks rather than intense satellites peaks indicate that there are no impurities of CuO and $Cu(OH)_2$ in Cu_2O films. Two peaks at 932.1 eV and 952.0 eV are attributed to $Cu2p_{3/2}$ and $Cu2p_{1/2}$ of Cu_2O, respectively. Two deconvoluted peaks in O1s spectrum (Fig. 5b) at 530.2 and 531.5 eV are attributed to Cu_2O and adsorbed hydroxide (–OH), respectively. The high-resolution W 4f core-level spectra (Fig. 5c) shows only paired sharp peaks at a binding energy of 35.5 and 37.7 eV, corresponding to the characteristic W $4f_{7/2}$ and W $4f_{5/2}$ peaks for WO_3, respectively.[16,35] It indicates that the tungsten (W) is fully oxidized and only presented as the six-valent oxidation state (W^{6+}) in the film. The O 1s core level XPS spectrum (Fig. 5d) also contains one main peak at low binding energy and additional peaks at high binding energies, 530.3 and 531.4 eV, originated from the oxygen bond with W atoms (W–O) in the crystal structure and the surface-adsorbed -OH bond, respectively.[16] The binding energies of 159.4 and 164.7 eV in Bi 4f core-level spectrum (Fig. 5e) are attributed to the $4f_{7/2}$ and $4f_{5/2}$ of Bi^{3+}, respectively.[36] It indicates that Bi element was successfully doped with the oxidation state of Bi^{3+} in the WO_3 film.

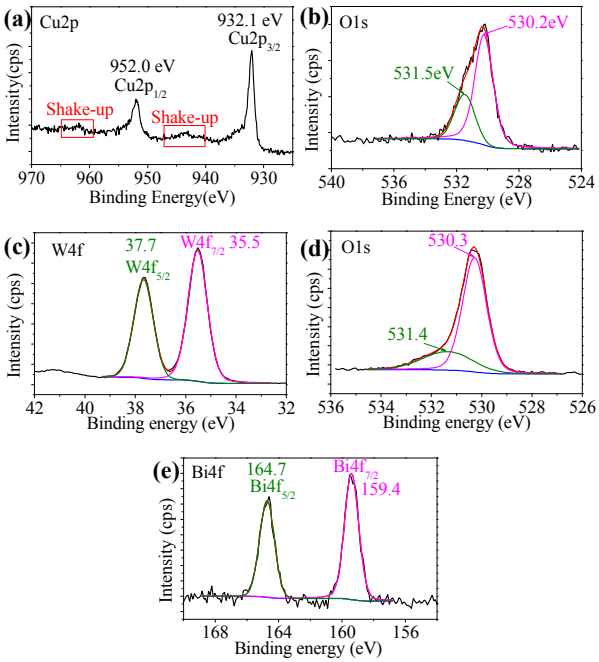

Fig. 5 The typical XPS spectra of (a) Cu2p and (b) O1s of Cu_2O/FTO films, and (c) W4f, (d) Bi4f and (e) O1s of Bi-WO_3 film. The black curves correspond to the experimental data, and they were fitted with the colored curves using an XPS fitting program (XPSPEAK41).

View Article Online
DOI: 10.1039/C6NJ02432G

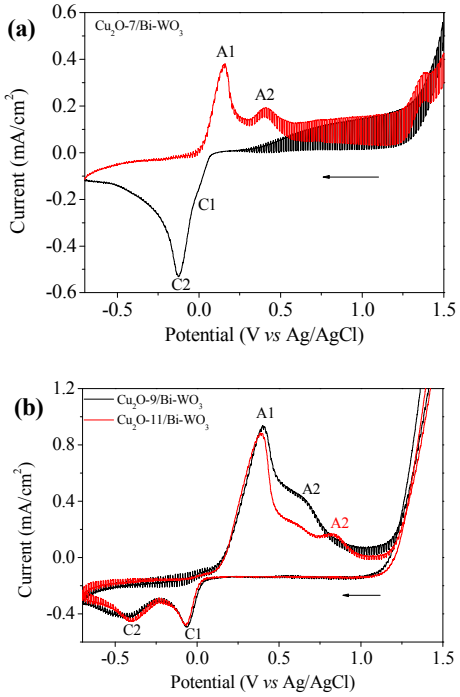

Fig. 6 Cyclic voltammograms for (a) the Cu_2O-7/Bi-WO_3 and (b) Cu_2O-9/Bi-WO_3 and Cu_2O-11/Bi-WO_3 electrodes in 0.5 M Na_2SO_4 electrolyte solution (scan rate: 10 mV/s) under the chopped 1 sun illumination. Black arrows show scan direction.

Cyclic voltammograms (Fig. 6) were obtained under the chopped 1 sun light illumination to evaluate the photochemical water splitting activity and the surface stability of Cu_2O/Bi-WO_3 bilayer films. The corresponding values of anodic peaks and cathodic peaks are shown in Table 1. Recently, the PEC water splitting activity of the n-WO_3, p-Cu_2O, and n-WO_3/p-Cu_2O bilayer photoelectrodes was evaluated by Minggu *et al.*[24] via linear scan voltammetry (LSV) method under Xenon light illumination. Fig. 6a shows that Cu_2O film has two anodic peaks and two cathodic peaks in CV of Cu_2O-7/Bi-WO_3 bilayer film. The first anodic peak (A1) at 0.16 V corresponds to the oxidation of Cu_2O to CuO; the second anodic peak (A2) at 0.41 V corresponds to the dissolution of CuO to Cu^{2+}. The first cathodic peak (C1) at -0.01 V corresponds to the reduction of Cu^{2+} to CuO; the second cathodic peak (C2) at -0.12 V corresponds to the reduction of CuO to Cu_2O.[37] For Cu_2O-9/Bi-WO_3 and Cu_2O-11/Bi-WO_3 (Fig. 6b), anodic peaks (A1 and A2) and cathodic peaks shifted to more positive and more negative than that of Cu_2O-7/Bi-WO_3; it indicates that it needs more potential energy to oxidize or reduce those two films, which are attributed to the film characteristics with relatively high crystallinity. However, the whole anodic current areas of these two films are much larger than their corresponding cathodic current areas. This indicates that these two films will be easily dissolved at an applied positive potential. It is easily observed that only Cu_2O-7/Bi-WO_3 shows the best performance of the anodic photocurrent while Cu_2O-9/Bi-WO_3 and Cu_2O-11/Bi-WO_3 show very low anodic photocurrent and low cathodic photocurrent. One possible reason can be given for this phenomenon. In the process for deposition of Cu_2O film in the solution with high pH, the slow dissolution of WO_3(s) to WO_4^{2-}(aq) would give a competition with the deposition of Cu_2O even it was very weak. Therefore, the interface formed at different pH value will be different.

Table 1 Anodic peaks (A1, A2) and cathodic peaks (C1, C2) in CVs of Cu_2O-7/Bi-WO_3, Cu_2O-9/Bi-WO_3, and Cu_2O-11/Bi-WO_3 electrodes in 0.5 M Na_2SO_4 electrolyte solution as shown in Fig. 6.

Films	A1 (V)	A2 (V)	C1 (V)	C2 (V)
Cu_2O-7/Bi-WO_3	0.16	0.41	-0.01	-0.12
Cu_2O-9/Bi-WO_3	0.41	0.63	-0.07	-0.40
Cu_2O-11/Bi-WO_3	0.39	0.83	-0.06	-0.42

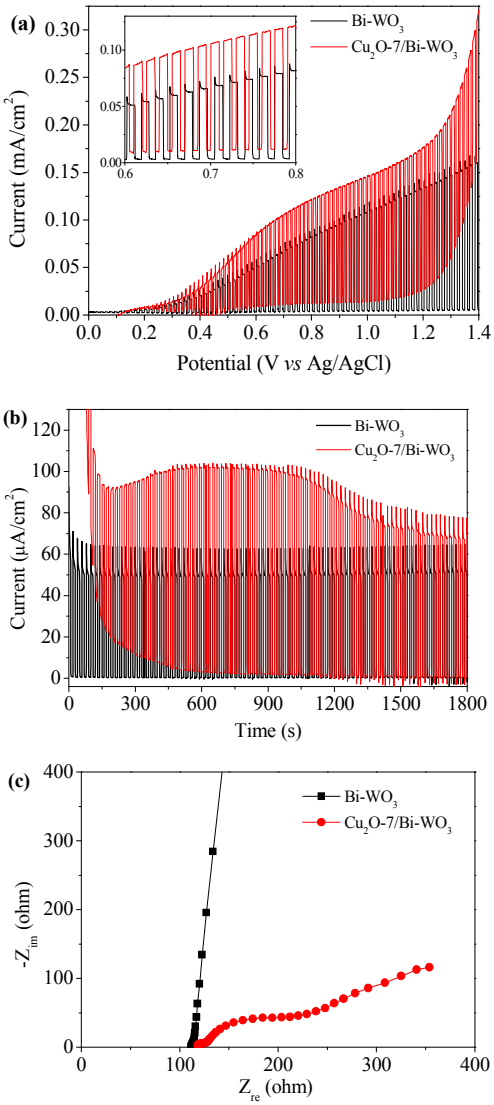

Fig. 7 (a) Photocurrents and (b) stability measurements at +0.65 V of Bi-WO_3 film (black color) and Cu_2O-7/Bi-WO_3 film (red color) measured in 0.5 M Na_2SO_4 electrolyte solution under chopped 1 sun illumination. (c) Electrochemical impedance spectra (EIS) of Bi-WO_3 film and Cu_2O-7/Bi-WO_3 film at E_{oc} under 1 sun illumination.

View Article Online
DOI: 10.1039/C6NJ02432G

To know the PEC performance of the Cu_2O-7/Bi-WO_3 bilayer film, the photocurrent of the bare Bi-WO_3 film was also checked and compared as shown in Fig. 7a. Herein, the thermodynamic potential for water oxidation is about 0.65 V vs Ag/AgCl at pH = 6.3.[16] The photocurrents of the bare Bi-WO_3 electrode and Cu_2O-7/Bi-WO_3 electrodes are *ca*. 54.7 and 85.7 $\mu A/cm^2$, respectively, at the applied potential value of 0.65 V vs Ag/AgCl; the anodic photocurrent of Bi-WO_3 thin film was improved by 56.67% after electrodeposition of thin Cu_2O film at pH 7. To confirm the improvement of anodic photocurrent is caused by the Cu_2O-7/Bi-WO_3 heterojunction rather than the anodic photocurrent from Cu_2O layer, the photocurrent response of Cu_2O-7 film in the potential range of 0 to 1.4 V *vs* Ag/AgCl was also checked at the same condition as shown in Fig. S10g (ESI†). it shows no anodic photocurrent response in the high positive potential range and only cathodic photocurrent response near the negative potential. Therefore, the enhanced anodic photocurrent of Cu_2O-7/Bi-WO_3 electrode is caused by the formation of heterojunction, not by Cu_2O layer. The photocurrent of the bare Bi-WO_3 film always shows an initial anodic photocurrent spike before a steep decay to a steady-state photocurrent at the moment of turning the light on as shown in the inset of Fig. 7a. It is mainly attributed to the significant electron/hole recombination at the instantaneous time. After coupling with Cu_2O thin layer, the spikes are disappeared at the applied potential more than 0.6 V vs Ag/AgCl. It indicates that electron-hole recombination can be sufficiently suppressed when the p-n junction formed.

Because the redox potentials for the reduction and oxidation of Cu_2O lie within its bandgap, it can be easily corroded in aqueous solutions under light illumination.[19,38,39] The dark current of the Cu_2O-7/Bi-WO_3 is higher than the bare Bi-WO_3 and sharply raises after *ca*. 1.3 V as shown in Fig. 7a. Two plausible explanations for this case are that: (1) photo-corrosion and oxidation of Cu_2O is happened; (2) electrochemical oxidation of water by Bi-WO_3 film becomes easier after combined with Cu_2O layer. To evaluate the photocurrent stability of the films, the current-time curves of Bi-WO_3 and Cu_2O-7/Bi-WO_3 films were measured at a constant potential of 0.65 V vs Ag/AgCl under chopped 1 sun light as shown in Fig. 7b. In addition, the photocurrent of the Bi-WO_3 film was also checked under a continue illumination as shown in Fig. S9 (ESI†). The photocurrent of Bi-WO_3 film gradually decreases for the first around 100 seconds and then keeps stable for the rest of the time. The decay of the photocurrent is possibly caused by accumulation of the holes in the Bi-WO_3 space charge layer under prolonged irradiation, electron-hole recombination, and the initial unstable surface of Bi-WO_3.[40] For Cu_2O-7/Bi-WO_3 film, the high anodic current is caused by the partially surface oxidation and dissolution of Cu_2O layer for the first around 150 seconds. After that, the enhanced photocurrent occurs and then decays after 900s. This photocurrent decay indicates the continually surface oxidation and dissolution of Cu_2O layer, which is possibly caused by the decrease of the pH of the electrolyte according to the following reaction (3).

$$H_2O + 4h^+ \rightarrow O_2 + 4\ H^+ \qquad (3)$$

Although the photocurrent of Bi-WO_3 can be enhanced by the formation of the p-Cu_2O/n-Bi-WO_3 heterojunction, the Cu_2O is not so stable in PEC system. This chemical instability is an inherent drawback of Cu_2O. The other work will be done to improve the photostability of Cu_2O.

To determine the difference between Bi-WO_3 and Cu_2O-7/Bi-WO_3 electrodes, their interfacial charge-transfer resistances (R_{ct}) are checked at E_{oc} under 1 sun light illumination as shown in Fig. 7c. The semicircular feature of the EIS at high frequencies is the defining characteristic of the charge transfer process where the diameter of the semicircle is equal to the charge transfer resistance (R_{ct}).[41] The diameter of arc radius on the EIS Nynquist plot of the Cu_2O-7/Bi-WO_3 is much smaller than of Bi-WO_3, which indicates that the Cu_2O-7/Bi-WO_3 surface facilitates the transfer of photo-generated holes from the Cu_2O-7/Bi-WO_3 surface to the electrolyte solution.[42] In addition, the cathodic photocurrents of different films are also compared in the applied potential range of -0.6 to +0.2 V as shown in Fig. S10a-f (ESI†). The cathodic photocurrents of Cu_2O/Bi-WO_3 are smaller than those of pure Cu_2O films. This indicates that the heterojunction cannot effectively enhance their cathodic photocurrents. In addition, the photocurrents of the films prepared with stirring in the electrodeposition process are similar with those without stirring as shown in Fig. S11. The stirring has only a limited effect on the PEC performance of the films in our deposition system. Therefore, in this work, the Cu_2O/Bi-WO_3 bilayer heterojunction film mainly show photoanodic properties and its charge transfer mechanism in PEC system under 1 sun solar light illumination should follow the process as shown in Scheme 1a.

4. Conclusions

In this paper, Cu_2O thin layer was electrodeposited on the Bi-doped WO_3 thin film prepared by the simple spin-coating method. These thin bilayer films on FTO substrates show high transmittance in the range of visible light. The photoelectrochemical properties of Cu_2O/Bi-WO_3 bilayer films depend on the pH of the solution for electrodeposition. The Cu_2O/WO_3 bilayer photoelectrode obtained at pH 7 shows better anodic photocurrent than those obtained at pH 9 and 11. The photocurrent of the bare Bi-WO_3 film can be enhanced after construction of the p-Cu_2O/n-Bi-WO_3 heterojunction. The stability of the p-Cu_2O/n-Bi-WO_3 is not so stable, owing to the inherent instability of Cu_2O. However, this paper can give an extended interpretation on Cu_2O/WO_3 bilayer heterojunction. The methods for fabricating Cu_2O and WO_3 layers can be individually used to make the other bilayer structures.

Notes and references

1. S. J. A. Moniz, S. A. Shevlin, D. J. Martin, Z.-X. Guo and J. Tang, *Energy Environ. Sci.*, 2015, **8**, 731-759.
2. T. Hisatomi, J. Kubota and K. Domen, *Chem. Soc. Rev.*, 2014, **43**, 7520-7535.

View Article Online
DOI: 10.1039/C6NJ02432G

3. F. E. Osterloh, *Chem. Soc. Rev*., 2013, **42**, 2294-2320.
4. H. M. Chen, C. K. Chen, R.-S. Liu, L. Zhang, J. Zhang and D. P. Wilkinson, *Chem. Soc. Rev*., 2012, **41**, 5654-5671.
5. A. Kudo and Y. Miseki, *Chem. Soc. Rev*., 2009, 38, 253-278.
6. A. U. Pawar, C. W. Kim, M. J. Kang, Y. S. Kang, *Nano Energy*, 2016, **20**, 156-167.
7. C. W. Kim, Y. S. Son, M. J. Kang, D. Y. Kim, Y. S. Kang, *Adv. Energy Mater*., 2016, **6**, 1501754.
8. C. W. Kim, S. J. Yeob, H.-M. Cheng, Y. S. Kang, *Energy Environ. Sci*., 2015, **8**, 3646-3653.
9. J. Hong, W. Zhang, J. Ren and R. Xu, *Anal. Methods*, 2013, **5**, 1086-1097.
10. J. H. Kima, G. Mageshb, H. J. Kangc, M. Banu, J. H. Kim, J. Lee, J. S. Lee, *Nano Energy*, 2015, **15**, 153-163.
11. A. Goeppert, M. Czaun, J.-P. Jones, G. K. S. Prakash and G. A. Olah, Chem. Soc. Rev., 2014, **43**, 7995-8048
12. M. M. Najafpour, A. N. Moghaddam, S. I. Allakhverdiev and Govindjee, *Biochim. Biophys. Acta*, Bioenerg., 2012, **1817**, 1110.
13. X. Liu, F. Wang and Q. Wang, *Phys. Chem. Chem. Phys*., 2012, **14**, 7894–7911.
14. C. A. Bignozzi, S. Caramori, V. Cristino, R. Argazzi, L. Meda and A. Tacca, *Chem. Soc. Rev*., 2013, **42**, 2228–2246.
15. T. Zhu, M. N. Chong and E. S. Chan, *ChemSusChem*, 2014, 7, 2974–2997.
16. J. Y. Zheng, G. Song, J. Hong, T. K. Van, A. U. Pawar, D. Y. Kim, C. W. Kim, Z. Haider and Y. S. Kang, *Cryst. Growth Des*., 2014, **14**, 6057–6066.
17. J. Y. Zheng, Z. Haider, K. T. Van, A. U. Pawar, M. J. Kang, C. W. Kim and Y. S. Kang, *CrystEngComm*, 2015, **17**, 6070-6093.
18. M. A. Butler, *J. Appl. Phys*. 1977, **48**, 1914– 1920.
19. J. Y. Zheng, G. Song, C. W. Kim and Y. S. Kang, *Electrochimica Acta*, 2012, **69**, 340-344.
20. Q. P. Chen, J. H. Li, X. J. Li, K. Huang, B. X. Zhou, W. M. Cai and W. F. Shangguan, *Environ. Sci. Technol.*, 2012, **46**, 11451– 11458.
21. R. H. Coridan, M. Shaner, C. Wiggenhorn, B. S. Brunschwig and N. S. Lewis, *J. Phys. Chem. C*, 2013, **117**, 6949– 6957.
22. H. Wang, T. Deutsch and J. A. Turner, *J. Electrochem. Soc*., 2008, **155**, F91-F96.
23. T. Zhang, Z. Zhu, H. Chen, Y. Bai, S. Xiao, X. Zheng, Q. Xue and S. Yang, *Nanoscale*, 2015, **7**, 2933-2940.
24. L. J. Minggu, K. H. Ng, H. A. Kadir and M. B. Kassim, *Ceram. Int*., 2014, **40**, 16015-16021.
25. J. Y. Zheng, T.-K. Van, A. U. Pawar, C. W. Kim and Y. S. Kang, *RSC Adv*., 2014, **4**, 18616-18620.
26. M. Wang, L. Sun, Z. Lin, J. Cai, K. Xie and C. Lin, *Energy Environ. Sci*., 2013, **6**, 1211-1220.
27. Z. Kang, X. Yan, Y. Wang, Z. Bai, Y. Liu, Z. Zhang, P. Lin, X. Zhang, H. Yuan, X. Zhang and Y. Zhang, *Sci. Rep*., 2015, **5**, 7882.
28. P. Li, H. Jing, J. Xu, C. Wu, H. Peng, J. Lu and F. Lu, *Nanoscale*, 2014, **6**, 11380-11386.
29. D. Sharma, S. Upadhyay, A. Verma, V. R. Satsangi, R. Shrivastav and Sahab Dass, *Thin Solid Films*, 2015, **574**, 125-131.
30. C. C. Hu, J. N. Nian and H. Teng, *Sol. Energy Mater. Sol. Cells*, 2008, **92**, 1071-1076.
31. S. Wei, Y. Ma, Y. Chen, L. Liu, Y. Liu and Z. Shao, *J. Hazard. Mater*., 2011, **194**, 243-249.
32. J. Y. Zheng, A. P. Jadhav, G. Song, C. W. Kim and Y. S. Kang, *Thin Solid Films*, 2012, **524**, 50–56.
33. J. Y. Zheng, G. Song, C.W. Kim and Y. S. Kang, *Nanoscale*, 2013, **5**, 5279-5282.
34. J. E. Yourey and B. M. Bartlett, *J. Mater. Chem*., 2011, **21**, 7651-7660.
35. G. Wang, Y. Ling, H. Wang, X. Yang, C. Wang, J. Z. Zhang and Y. Li, *Energy Eviron. Sci*., 2012, **5**, 6180– 6187.
36. J. Wu, F. Duan, Y. Zheng and Y. Xie, *J. Phys. Chem. C*, 2007, **111**, 12866-12871.
37. L. L. Wu, L. K. Tsui, N. Swami and G. Zangari, *J. Phys. Chem. C*, 2010, **114**, 11551-1156.
38. A. Paracchino, V. Laporte, K. Sivula, M. Gratzel and E. Thimsen, *Nat. Mater*., 2011, **10**, 456 – 461.
39. X. Chang, T. Wang, P. Zhang, Y. Wei, J. Zhao and J. Gong, *Angew. Chem. Int. Ed*., 2016, **55**, 8840–8845.
40. F. F. Abdi and R. van de Krol, *J. Phys. Chem. C*, 2012, **116**, 9398–9404.
41. Z. Zhang, R. Dua, L. Zhang, H. Zhu, H. Zhang and P. Wang, *ACS Nano*, 2013, **7**, 1709–1717.
42. A. A. Dubale, C.-J. Pan, A. G. Tamirat, H.-M. Chen, W.-N. Su, C.-H. Chen, J. Rick, D. W. Ayele, B. A. Aragaw, J.-F. Lee, Y.-W. Yang and B.-J. Hwang, *J. Mater. Chem. A*, 2015, **3**, 12482-12499.

View Article Online
DOI: 10.1039/C6NJ02432G

Graphic Abstract

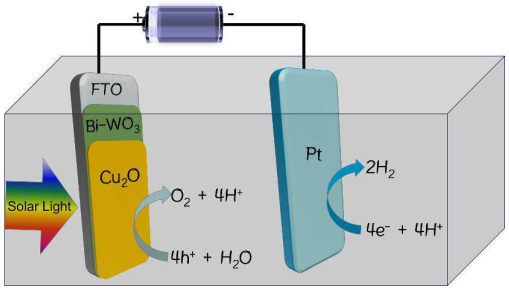

Cu_2O/Bi-WO_3 p-n heterojunction film as a photoanode can effectively separate photo-generated electron-hole for water oxidation.